Results in Physics 68 (2025) 108091

Contents lists available at ScienceDirect

Results in Physics

journal homepage: www.elsevier.com/locate/rinp

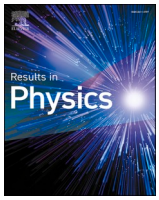

Compact low-noise GeV-scale electron-positron pair spectrometer

Jaehyun Song [a,d], Youhwan Noh [a], Mohammad Mirzaie [b,c], Calin Ioan Hojbota [b], Hyeong-il Kim [a], Seongmin Lee [a], Junho Won [a,e], Chiwan Song [a], Woosuk Bang [a,*]

[a] Department of Physics and Photon Science, GIST, Gwangju 61005, Korea
[b] Center for Relativistic Laser Science, Institute for Basic Science, Gwangju 61005, Korea
[c] Advanced Photonics Research Institute, GIST, Gwangju 61005, Korea
[d] Institute for Rare Isotope Science, Institute for Basic Science, Daejeon 34000, Korea
[e] Center for Exotic Nuclear Studies, Institute for Basic Science, Daejeon 34126, Korea

ARTICLE INFO

Keywords:
Electron-positron pair
Pair production
Pair spectrometer
Laser-plasma
Laser wakefield acceleration

ABSTRACT

Recent studies have successfully demonstrated a high-flux GeV-scale gamma-ray spectrometer using energy spectra of electron–positron pairs generated in a high-Z converter. In a confined space of a meter, resolving GeV-scale pair particles using a permanent magnet is challenging owing to its relatively weak magnetic field strength of around 1 T. In this study, we present a compact low-background GeV-scale electron–positron pair spectrometer design, utilizing permanent magnets and imaging plates, and its experimental validation. We investigated the arrangement of magnet blocks using Geant4 simulations to enhance energy resolution over a wide spectral range from MeV to GeV. An asymmetrical yoke design was implemented to maximize the bending power without obstructing particle trajectories. We utilized and evaluated the pair spectrometer system in pair-production experiments using a multi-petawatt laser, successfully detecting GeV-range electron–positron pair particles. Additional Geant4 simulations were conducted to validate the spectrometer's performance. This research contributes to the advancement of experimental capabilities in particle physics, especially for gamma-ray spectrometers in space-constrained environments.

Introduction

Permanent dipole magnets are widely used in experimental applications involving charged particle beams. Specifically, they are widely used in mass spectroscopy [1–5] and particle physics [6–11] for their compact size and relatively low cost compared with electromagnets. In laser-plasma experiments where space is often limited, magnetic spectrometers are used to analyse charged particles such as laser wakefield accelerated electrons. Several research groups have used permanent magnets as pair spectrometers to simultaneously obtain the energy spectra of electrons and positrons produced via Bethe-Heitler process using lasers [12–18].

Recent studies have proposed and demonstrated a high-flux GeV-scale gamma-ray spectrometer using the measured energy spectra of electron–positron pairs generated from gamma ray and high-Z converter interaction [19,20]. In these simulations and experiments, the incident gamma rays are converted to pair particles, which are collimated into a beam. This beam is deflected through a magnetic field and forms a spectral signal at the detector. The energy spectrum of the initial gamma ray is obtained by deconvolving the pair-particle spectra using the Bethe-Heitler cross-section [19–22]. Cavanagh *et al.* [20] noted that the uncertainty in the gamma-ray spectrum is mainly attributed to the measurement of the energy spectra of the electron–positron pairs, necessitating a pair spectrometer system with a wide spectral range and high resolution for the potential development of an accurate gamma-ray spectrometer. However, distinguishing GeV-scale pair particles from the remaining gamma rays after the conversion and collimation processes is a challenging task when using a permanent magnet in a confined space because of its relatively weak magnetic field strength of around 1 T.

In this paper, we present a novel, compact pair spectrometer, specifically designed for detecting GeV range electron–positron pairs, using a permanent dipole magnet and imaging plates (IPs), as well as its experimental validation. Monte Carlo simulations using Geant4 were performed during the design process to estimate pair particle trajectories and detector signal distributions, ensuring that particles with specific energies are detected at desired locations. Additionally, we utilized

* Corresponding author.
E-mail address: wbang@gist.ac.kr (W. Bang).

https://doi.org/10.1016/j.rinp.2024.108091
Received 17 May 2024; Received in revised form 6 December 2024; Accepted 15 December 2024
Available online 17 December 2024

Geant4 to simulate pair-production experiments using the spectrometer, which involved the bremsstrahlung and Bethe-Heitler processes occurring in high-Z targets. We compare the simulation results with the experimental data to confirm the validity of our spectrometer design.

Fig. 1 depicts our pair spectrometer schematic, including two lead collimators, a permanent dipole magnet, and two imaging plates. They are aligned so that the optical axis passes through the center of every component and aperture. A two-collimator setup is known to be suitable for minimizing the background on the detectors when measuring GeV-scale electron–positron pairs [19]. The first collimator is a 20-cm thick lead block with a 2-cm diameter hole. The second collimator consists of a lead cylinder with a 4-cm-diameter hole, coated with 1-cm-thick stainless steel, resulting in an effective inner diameter of 2 cm. The purposes of the stainless-steel coating were to assist in the collimation of radiation with lead and to avoid direct exposure to lead. The two collimators accept pair particles with a divergence angle of less than 16 mrad coming from the center of the converter back surface. The collimators were surrounded by at least 40 cm of lead shielding to protect the spectrometer, though this shielding is omitted from Fig. 1 to simplify the illustration. To detect the pair particles after passing through the 40-cm, 0.75 T magnet, a 20-cm-long, 4.5-cm-wide IP (Fuji-BAS-MS) is installed 1 cm away from the magnet exit for the detection of pair particles with energies above 200 MeV. Another 40-cm-long, 4.5-cm-wide IP (Fuji-BAS-MS) is placed 47 cm away from the magnet to measure particles with kinetic energies exceeding 300 MeV, providing a better separation from the gamma rays. Among every spectrometer component, the permanent magnet was specifically designed to reduce the background noise and to detect a wide spectral range from MeV to GeV.

Magnet design for a compact low-background pair spectrometer

For the design of a spectrometer magnet, it is important to consider the trade-offs between widening the magnet gap for background reduction and the corresponding decrease of the magnetic field strength in the gap. The gap between the north and the south poles must be sufficiently large enough to accommodate high-energy pair particles, as these particles can generate significant background on the spectrometer through secondary radiations when they strike the frame of the magnet. In our setup illustrated in Fig. 1, we used two lead collimators with a 2-cm-diameter aperture to select electrons, positrons, and gamma photons with a divergence angle of less than 16 mrad. In order to reduce the secondary radiations from the frame, the spectrometer has a magnet gap of 4 cm. (See Supplementary Fig. S1 to see the quantitative analysis of the background noise reduction for different magnet gaps.) To compensate for the decrease of the magnetic field strength due to the wide gap, a high-grade magnet, NdFeB-N52, was chosen as the magnetic flux source.

As typical pair-particle beams converted from gamma-ray beams have their inherent divergence [23], the average divergence angle of

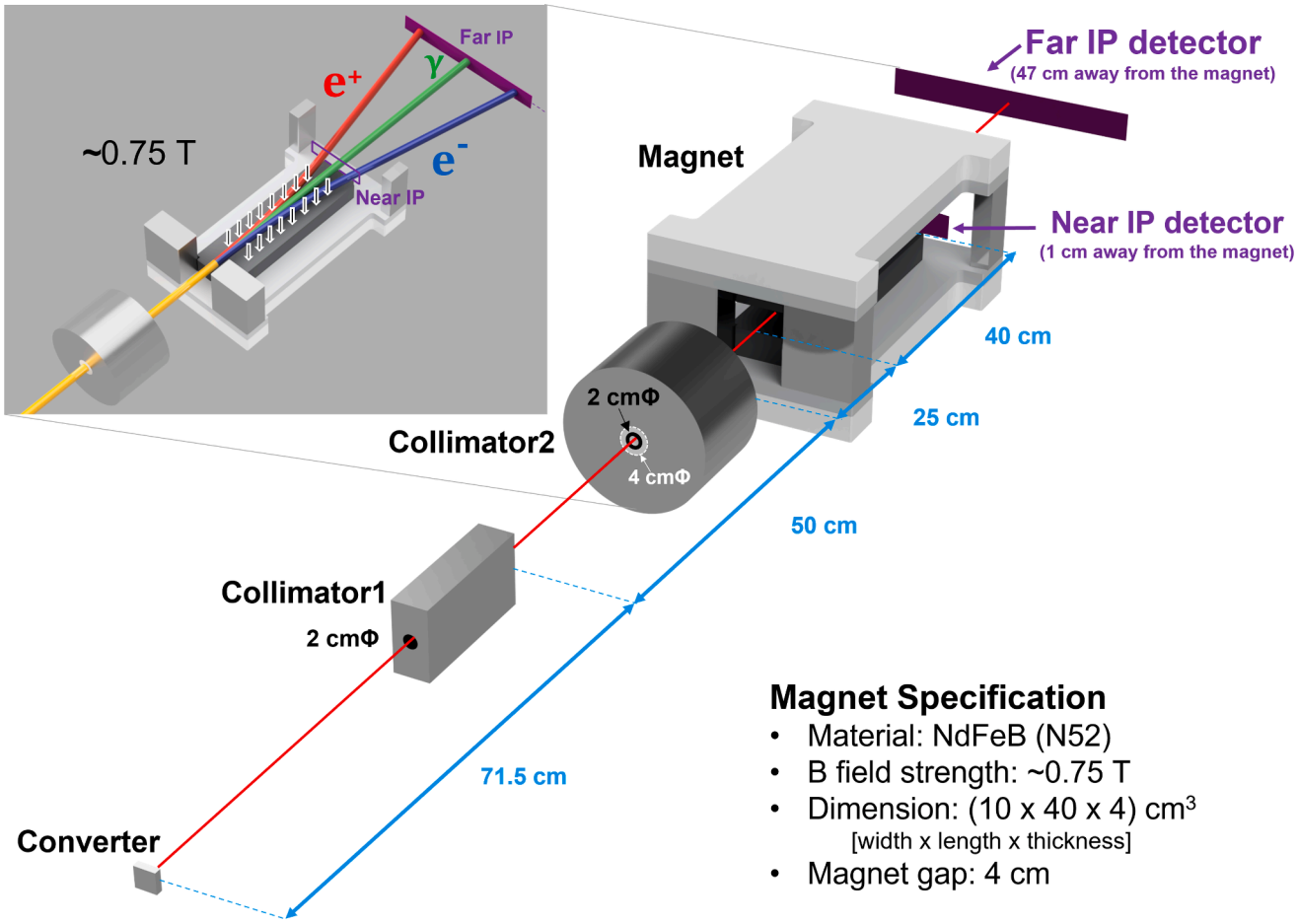

Fig. 1. Schematic of the pair spectrometer arrangement in the experiment. The pair spectrometer consists of two collimators, a permanent dipole magnet, and imaging plates. The first collimator is a 20-cm thick lead block with a 2-cm diameter hole. The second collimator is a 15-cm-thick lead cylinder with a 4-cm diameter hole coated with a 1-cm-thick layer of stainless steel (which results in an effective inner diameter of 2 cm). 10-cm-wide and 40-cm long magnetic dipoles are designed to have a 4-cm gap between the two poles. The 0.75 T magnet assembly has an asymmetrical yoke structure to maximize the detection energy range. The inset depicts the direction of the magnetic field and the resulting paths of electrons, positrons, and gamma rays. The near and far IPs are installed 1 cm and 47 cm behind the magnet, respectively, to detect the GeV-scale pair particles.

electron–positron pairs is inversely proportional to the Lorentz factor of each particle [16]. Consequently, pair-particle yields after collimation are often insufficient for long-range detection (See Supplementary Fig. S2 for the correlations between energy and angle, and Supplementary Fig. S3 for the fraction of positrons passing through the collimators as a function of energy). Hence, we aimed to distinguish GeV-scale pair particles from the unconverted gamma rays within a meter. Fig. 2(a) and 2(b) depict calculated trajectories of electrons with various kinetic energies when passing a uniform magnetic field area with different magnet arrangements. Both cases consist of two pairs of magnet blocks (10 cm × 20 cm) with a uniform magnetic flux density of 0.75 T, but with different arrangements: (a) a square and (b) a long rectangle. For simplicity, we assumed an ideal pencil beam along the propagation axis for trajectory calculations.

The upper limit of the detection energy range depends on whether the energetic charged particles can be separated from the remaining gamma rays. Thus, the deflection angle must be sufficiently large for the particles to be distinguished from the outermost collimated gamma rays at the detection plane. The black and red curves in Fig. 2(c) show the deflection angles of electrons after passing through a magnet in a square and a long rectangle shape, respectively. For the particles with energy higher than 365 MeV, the deflection angles after passing through a 10 cm × 40 cm magnet (red curve) are roughly twice the magnitude of those resulting from a 20 cm × 20 cm magnet (black curve). This is consistent with Fig. 2(a) and 2(b), where the path length in the magnetic field nearly doubles for particles with kinetic energy exceeding 365 MeV. The lower limit of the detection range is determined to be the energy of the particle that deflects 180° after passing the magnet. The

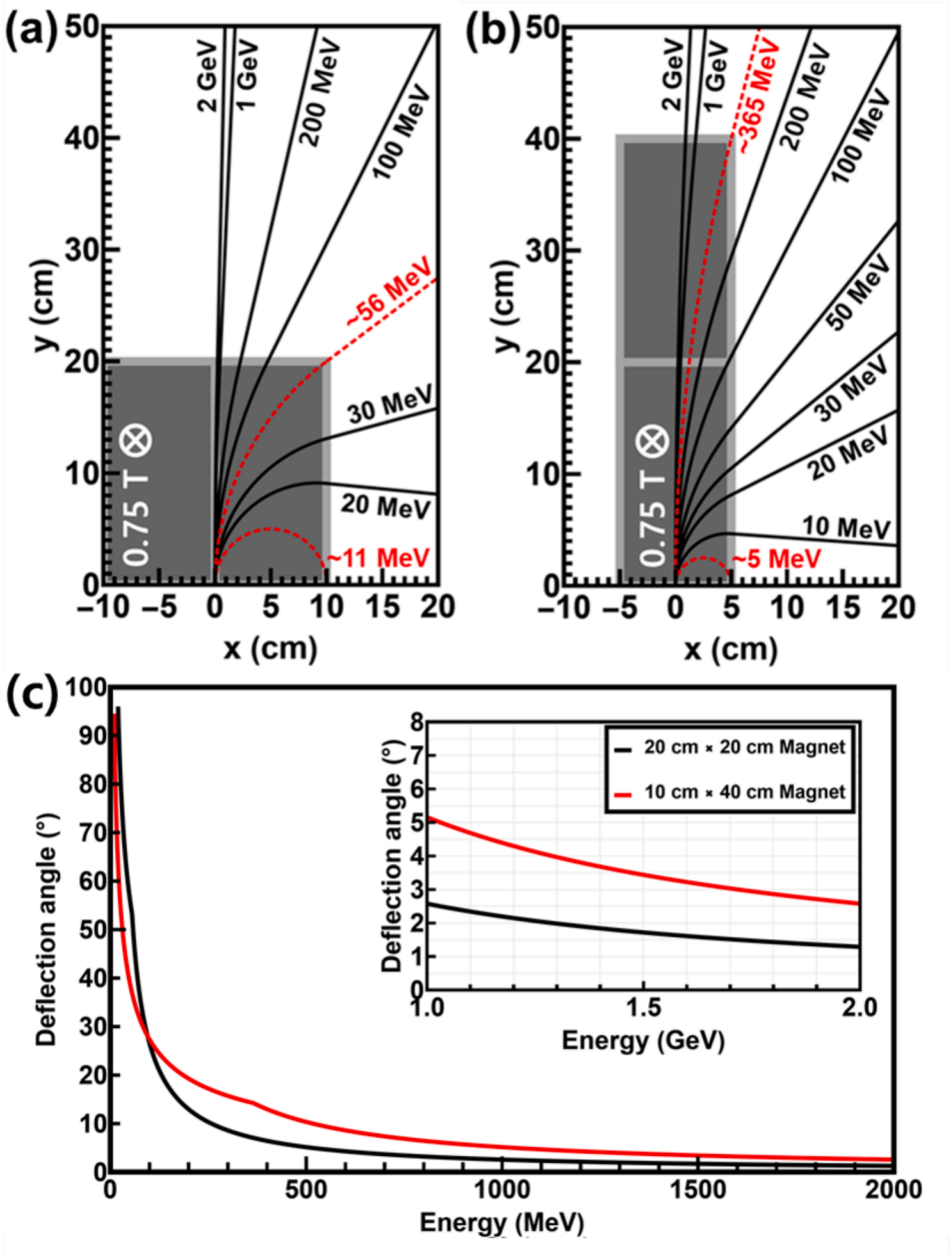

Fig. 2. Comparison of particle trajectories between different dipole magnet arrangements. Calculated trajectories of electrons with various kinetic energies when using (**a**) square (20 cm × 20 cm) and (**b**) rectangular arrangements (10 cm × 40 cm) of two pairs of magnet blocks (10 cm × 20 cm), assuming a uniform magnetic field of 0.75 T. The red dashed lines indicate trajectories passing the corner of the magnet. (**c**) Deflection angle as functions of kinetic energy. Black and red curves indicate the deflection angle of electrons after passing a uniform magnetic field of 0.75 T in square and rectangular shapes, respectively. (For interpretation of the references to colour in this figure legend, the reader is referred to the web version of this article.)

particle trajectory passes the corner of the magnet at the entrance part, which corresponds to 11 MeV and 5 MeV as described in red dashed lines in Fig. 2(a) and 2(b), respectively. A wide detection range from MeV to GeV level can be achieved by designing the permanent magnet longer in the beam propagation direction. The detection of GeV-scale pair particles is discussed further in detail with Fig. 4(b).

A practical issue in constructing this long magnet is the arrangement of yokes or a ferromagnetic frame without interfering with the trajectories of the particles. The function of a yoke is to provide the return path for magnetic flux and to secure stability of the system. Therefore, a certain cross-sectional area of the yoke is required for structural stability and high flux density [24,25]. Instead of blocking the entire side part of the magnet with a yoke as in conventional C-shaped and H-shaped magnets, we chose a yoke design of four posts at every corner of the magnet for a broad detection energy range. Fig. 3(a) shows the right half of a symmetrical yoke design with four 7 cm × 6 cm yokes at every corner. While this is a stable yoke design with a symmetrical field distribution, two of its yokes at the exit block pair particles with energy ranging from 140 to 500 MeV, as illustrated by the red lines in Fig. 3(a). The improved yoke design is asymmetrical, as shown in Fig. 3(b). The two yokes at the exit were placed 13 cm away from the central axis and thinned by 4 cm, while the yokes at the entrance got 4 cm thicker, maintaining the same total cross-sectional area. This unique yoke design permits pair particles above 5.2 MeV to be detected without encountering any obstructions. Even particles approaching the region marked by the red curves can be detected by strategically placing IPs within the ample space between the yokes and the magnetic field region.

We conducted a comparative analysis of the yoke positions in each magnet using Geant4 simulations (Geant4-10.7.1, PhysicsList: QGSP_BERT_HP), wherein electron–positron pair particles were directed toward the magnets. Fig. 3(c) and 3(d) show the simulated pair-particle signals when measured right behind the yokes at the exit of the magnet

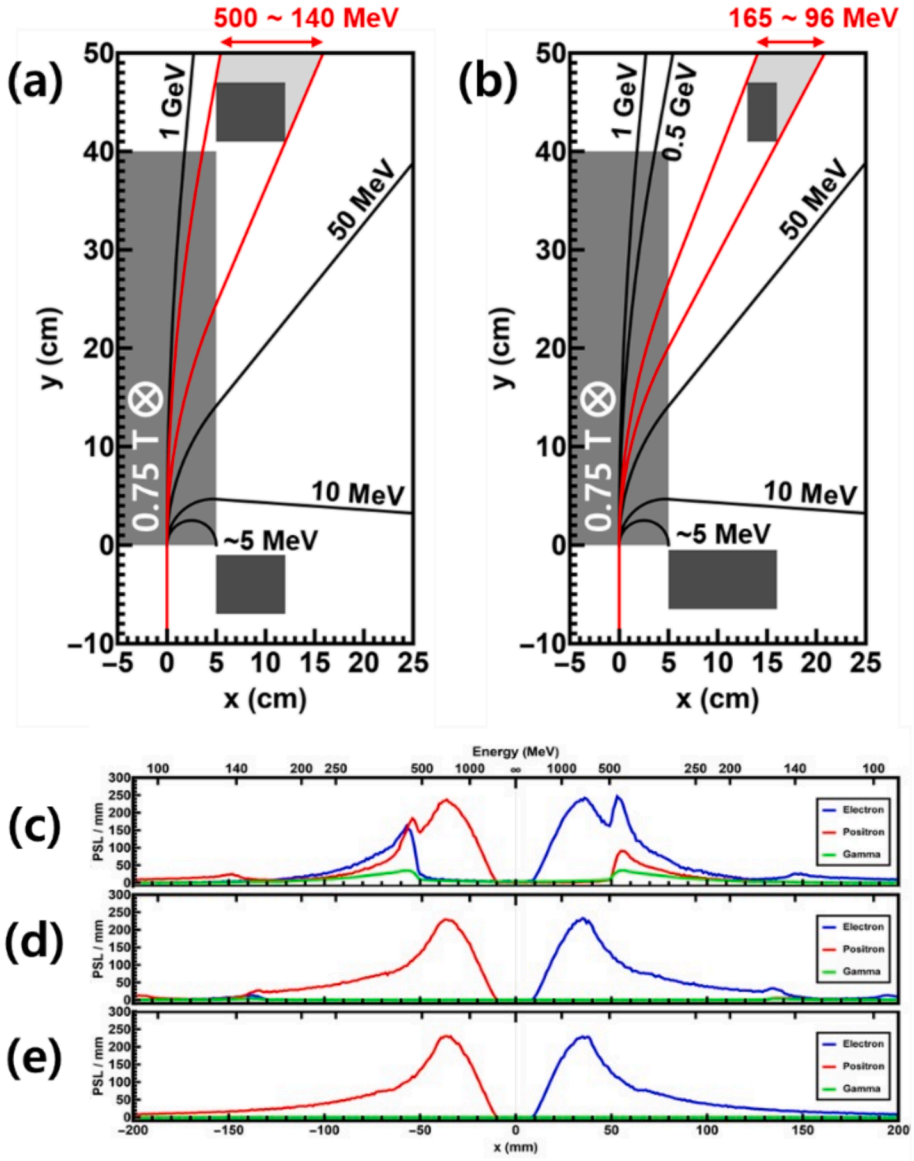

Fig. 3. Blocked energy range and secondary radiations in two different yoke designs. (**a**) Typical symmetric design with yokes at all four corners. The red curves indicate that electrons with energies ranging from 140 MeV to 500 MeV are blocked by one of the yokes. (**b**) The asymmetric version that blocks particles with a narrower energy range of 96 MeV to 165 MeV, as shown with red curves. Geant4-simulated spatial distribution of PSL values measured right behind the yokes at the exit of the magnet in (**c**) symmetrical and (**d**) asymmetrical yoke structures. (**e**) PSL distribution measured without the effect of yokes. The input beam is electron–positron pair particles with a constant spectrum from 5 MeV to 1 GeV collimated by a 2-cm-diameter aperture with a 16 mrad acceptance angle. (For interpretation of the references to colour in this figure legend, the reader is referred to the web version of this article.)

in the symmetrical and asymmetrical design, respectively. The input beam used in the simulation was electron–positron pair particles with a constant spectrum from 5 MeV to 1 GeV collimated by a 2-cm-diameter aperture with a 16-mrad acceptance angle. Fig. 3(e) depicts the expected spatial distribution of the input beam without the interaction with the yokes. In Fig. 3(c), scattered particles are distinctly visible near $x = \pm 55$ mm, corresponding to the positions of 400–500 MeV pair particles. This indicates that the yokes close to the trajectories of high-energy particles significantly influence the adjacent parts of the spectrum, contributing a considerable amount of secondary radiations (see Supplementary Fig. S4). The asymmetrical yoke design, as in Fig. 3(b), on the other hand, can reduce a significant amount of background while maintaining structural stability and magnetic flux density. For simplicity, the calculations and simulations in Fig. 3 were conducted using a uniform magnetic field and an ideal pencil-like pair particle beam along the propagation axis.

Experiments using the pair spectrometer

Adopting the extended magnet configuration and the asymmetrical yoke design, a permanent dipole magnet assembly was manufactured for a uniform magnetic flux density of 0.75 T at the center. Fig. 4(a) illustrates the distribution of magnetic flux density measured on a plane centered between the two magnetic pole units, using a three-dimensional colormap surface and projection. The surface has a camelback-like shape in the middle because each magnetic pole unit is the assembly of two 10 cm × 20 cm NdFeB-N52 blocks. The magnetic field distribution exhibits a modest degree of asymmetry because of the asymmetric yoke structure, but the overall distribution seems almost symmetrical. The average value of the magnetic flux density over the entire area of 10 cm × 40 cm is 0.59 T, with a standard deviation of 0.13 T. The central region of 2 cm × 40 cm ($-10\,\text{mm} \leq x \leq 10\,\text{mm}$) has an average magnetic flux density of 0.70 ± 0.08 T. In the subsequent simulations, we used three layers of magnetic field volumes using 2D field distributions measured on three planes: the middle plane as described in Fig. 4(a), along with two additional planes that were 1 cm above and below the middle plane.

We examined the location of the IP for the detection of GeV-range pair particles. IP is a film-type radiation detector that can detect electrons, positrons, and gamma rays. The fluence can be calculated using photostimulated luminescence (PSL) data obtained from the scanning process after the detection. Based on the measured magnetic field in

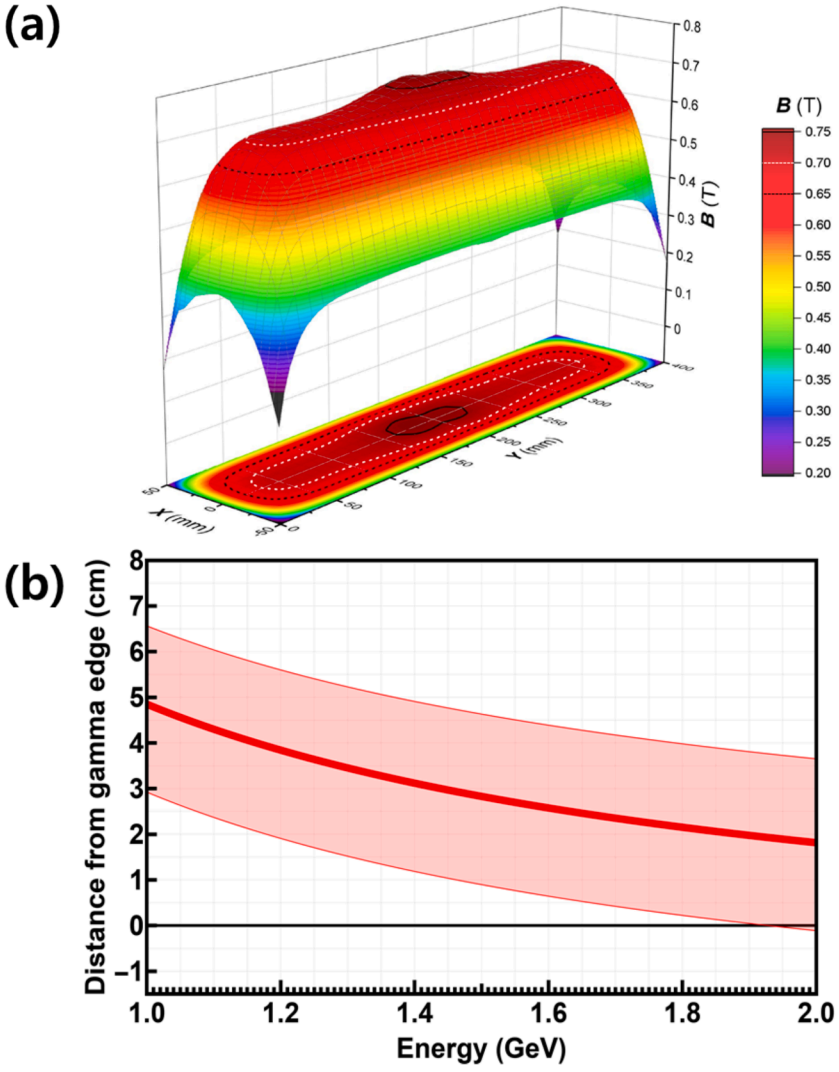

Fig. 4. Measured magnetic field and expected position of the pair-particle signals on the detector. (**a**) The magnetic field distribution using a 3D colormap surface and projection within a 10 cm × 40 cm region, measured on a plane centered between the two magnetic pole units. (**b**) Expected pair-particle position as a function of particle energy at the plane 50 cm away from the magnet. The position is expressed as the distance from the edge of the gamma-ray signal to examine the overlap between the pair particle and the gamma ray. The red line corresponds to the ideal pencil beam, whereas the shaded area corresponds to the collimated beam with a divergence less than 16 mrad. (For interpretation of the references to colour in this figure legend, the reader is referred to the web version of this article.)

Fig. 4(a) and the expected parameters of the collimated beam, we simulated the spatial distribution of the signal on the IP installed 50 cm away from the magnet. Given that we employ a gamma ray beam as the initial source for the pair-particle beam, it is crucial to determine the spatial detection range of the remaining gamma rays after the conversion at the IP to differentiate the pair-particle signals from the gamma-ray signals. Assuming a perfect shielding from our collimator setup, the edge of the gamma-ray signal at the IP is positioned 1.23 cm away from the center of the IP. We simulated the distance between the particle signal and the gamma-ray edge on the detection plane to determine the spectrometer's resolution to resolve high-energy particles. The maximum resolvable energy was approximately 2 GeV at 50 cm away, as shown in Fig. 4(b). The thick red line represents where the ideal pencil-like pair particle beam arrives after passing through the magnet. The shaded area corresponds to the signal from the pair particle beam with a divergence angle that falls within the acceptance angle (16 mrad) of our collimator setup. (See Supplementary Figs. S5 and S6 to find ΔE for a 1 mrad beam divergence and ΔE_{min} corresponding to a single IP pixel, respectively.) Using the compact spectrometer with the 40-cm-long magnet and the IP installed 50 cm away, GeV-scale pair particles can be separated from the remaining gamma rays.

Using our spectrometer system, pair production experiments [26,27] were carried out with a multi-petawatt laser at the Center for Relativistic Laser Science (CoReLS) [28]. The experimental configuration comprised two distinct parts. In the initial stage, a Laser Wakefield Acceleration (LWFA) was used to generate a high-energy electron beam [29]. This beam was subsequently directed onto a 4-mm thick lead plate and emitted bremsstrahlung gamma rays [26]. A 1.3 T magnet was used to deflect the charged particles to the sides, including those generated in the plate and the initial electrons that penetrated the plate. Only the bremsstrahlung gamma rays exited the vacuum chamber through a thin Mylar window. The purpose of the second part was to induce the production of electron–positron pairs through the irradiation of a 6-mm-thick lead converter using the high-energy gamma rays created in the first part. The pair production stage was placed in the air since the system is known to be insusceptible to the interaction of the pairs with air [19]. (See Supplementary Fig. S7 to see the effect of air on the beam divergence).

The resulting electron–positron pair particles and unconverted gamma rays went into the pair spectrometer system described in Fig. 1, and the pair particles were measured using the near and far IPs, as shown in Fig. 5(a) and 5(c). To eliminate the loss of PSL caused by ambient background lights, a 50-μm-thick black aluminum foil was used to encase each IP. The near and far IPs were scanned together for about 10 min after the acquisition of five consecutive measurements. The PSL data were calculated, taking the fading effects of the IP into account [30,31]. We conducted Geant4 simulations applying the experimental setup, the measured magnetic field, and the energy spectrum of the input LWFA electron beam as described in Figs. 1, 4(a), and 6(a), respectively, to verify the performance of the pair spectrometer. Fig. 5 (b) and 5(d) are Geant4-simulated PSL signals from the gamma rays and pair particles measured in the near and far IPs, respectively [32,33]. Separation of above-GeV pair-particle signals from the gamma-ray signals can be seen in Fig. 5(c) and 5(d).

Fig. 6(a) shows 6-shot-averaged LWFA electron beam spectrum measured using a 1.3 T magnet and Lanex screens inside the vacuum. The total charge above 320 MeV was 950 pC, with a local spectral peak at ~2.2 GeV. The spectrum was used in the simulations as the initial input beam for the bremsstrahlung gamma rays. Fig. 6(b) depicts the experimentally measured positron and electron spectra in red and blue lines, respectively. Only the spectra above 500 MeV were plotted because some particles with large divergence started to go out of the vertical limit of the far IP, reducing the signal below 500 MeV. Fig. 6(c) and 6(d) show the experimental and simulated particle spectra in black and red lines, respectively, where 6(c) is for positrons and 6(d) is for electrons (See Supplementary Fig. S3 for the expected energy spectrum of positrons at the rear surface). The measured magnetic field in Fig. 4(a) was applied in the simulations. The simulated results are in good agreement with the experimental data, validating that the pair spectrometer system successfully detected GeV-range electron–positron pair particles.

Conclusion

We presented an experimental measurement of pair particles using a compact, low-background pair spectrometer capable of detecting GeV-scale electron–positron pairs. We have significantly reduced the secondary radiations from the magnet frame by adopting a 4-cm magnet gap. Compared with a 2-cm gap, the signal-to-noise ratio improved by 300 times. (See Supplementary Fig. S1.) We have further reduced the

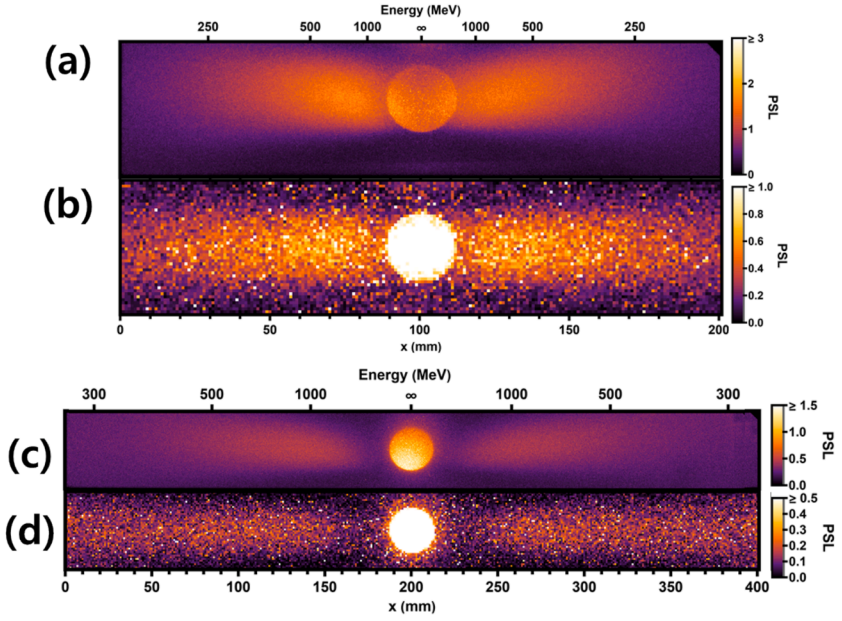

Fig. 5. Experimental gamma-ray and pair-particle signals measured on (**a**) the near IP and (**c**) the far IP. Geant4-simulated gamma-ray and pair-particle signals measured on (**b**) the near IP and (**d**) the far IP. In both cases, the near and far IPs are installed 1 cm and 47 cm away from the magnet, respectively.

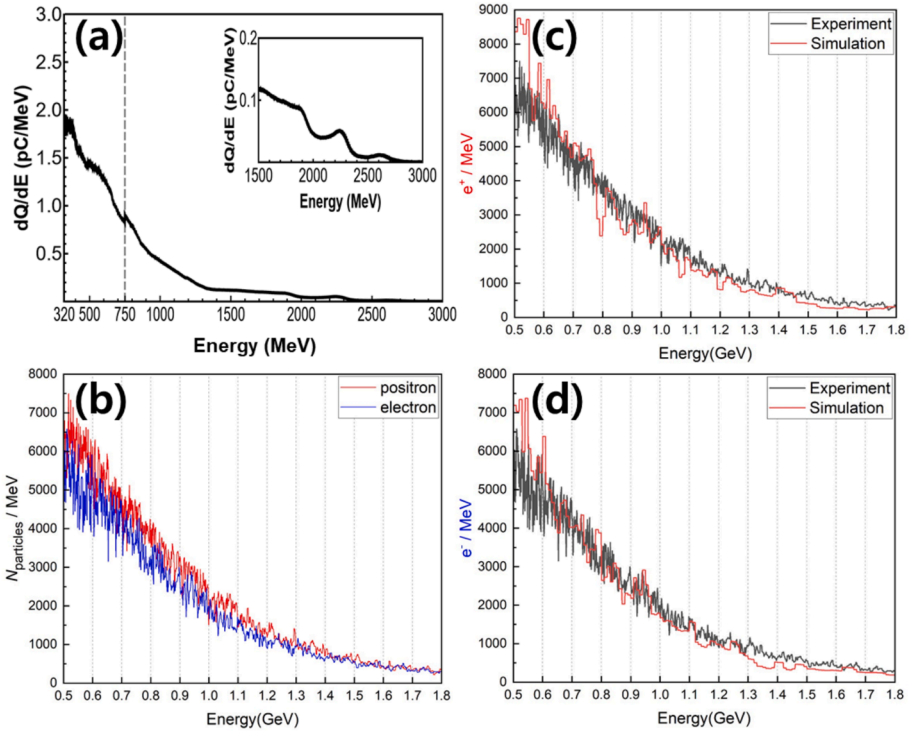

Fig. 6. Experimental and Geant4-simulated pair-particle spectra. (**a**) 6-shot-averaged LWFA electron beam spectrum experimentally measured using a 1.3 T magnet and Lanex screens inside the vacuum chamber. (**b**) Experimentally measured positron and electron spectra in red and blue lines, respectively. Comparison of (**c**) positron and (**d**) electron spectra between the experimental and simulated data in black and red lines, respectively. The simulated spectra are normalized so that their total numbers match the experimental results. All the pair-particle spectra were measured in the far IP for the particles above 500 MeV. (For interpretation of the references to colour in this figure legend, the reader is referred to the web version of this article.)

background noise by applying an asymmetrical yoke design. (See Supplementary Fig. S4 for details.) The challenges associated with weak magnetic field strength, due to an increased gap between the magnetic poles, were addressed by utilizing high-grade NdFeB-N52 magnets and extending the magnet blocks along the beam propagation direction. A unique asymmetrical yoke design further improved particle detection abilities without obstructing the high-energy pair-particle trajectories. In the pair-production experiments with a multi-petawatt laser at CoReLS, the spectrometer system successfully detected GeV-range electron–positron pair particles. The close agreement between the Geant4 simulations and the measured electron and positron spectra validated the performance of the spectrometer. This spectrometer configuration can significantly enhance experimental capabilities for gamma-ray spectrometry and pair particle detection, particularly in space-constrained environments, paving the way for more efficient and precise studies in laboratory astrophysics and in high-energy particle physics.

CRediT authorship contribution statement

Jaehyun Song: Writing – review & editing, Writing – original draft, Visualization, Validation, Software, Methodology, Investigation, Formal analysis. **Youhwan Noh:** Writing – review & editing, Methodology, Investigation. **Mohammad Mirzaie:** Writing – review & editing, Methodology, Investigation. **Calin Ioan Hojbota:** Writing – review & editing, Methodology, Conceptualization. **Hyeong-il Kim:** Writing – review & editing, Methodology, Investigation. **Seongmin Lee:** . **Junho Won:** Writing – review & editing, Methodology, Investigation. **Chiwan Song:** Writing – review & editing, Investigation. **Woosuk Bang:** Writing – review & editing, Supervision, Project administration, Conceptualization.

Declaration of competing interest

The authors declare that they have no known competing financial interests or personal relationships that could have appeared to influence the work reported in this paper.

Acknowledgments

This work was supported by the National Research Foundation of Korea (NRF) grant funded by the Korea government (MSIT) (No. 2023R1A2C1002912).

Appendix A. Supplementary data

Supplementary data to this article can be found online at https://doi.org/10.1016/j.rinp.2024.108091.

Data availability

Data will be made available on request.

References

[1] Zeller LC, Kennady JM, Campana JE, Kenttamaa H. Characterization of a small FTICR mass spectrometer based on a permanent magnet. Anal Chem 1993;65(15):2116–8.
[2] Diaz JA, Giese CF, Gentry WR. Portable double-focusing mass-spectrometer system for field gas monitoring. Field Anal Chem Technol 2001;5(3):156–67.
[3] Mauclaire G, Lemaire J, Boissel P, Bellec G, Heninger M. MICRA: a compact permanent magnet Fourier transform ion cyclotron resonance mass spectrometer. Eur J Mass Spectrom 2004;10(2):155–62.
[4] Li C, et al. Towards higher sensitivity of mass spectrometry: A perspective from the mass analyzers. Front Chem 2021;9:813359.
[5] Bergin M, et al. "Low-energy electron ionization mass spectrometer for efficient detection of low mass species,". Rev Sci Inst 2021;92(7).

[6] Kraus R, et al. The overview and history of permanent magnet devices in accelerator technology. IEEE Trans Magn 1994;30(4):1547–54.
[7] Cha HJ, et al. "Absolute energy calibration for relativistic electron beams with pointing instability from a laser-plasma accelerator,". Rev Sci Inst 2012;83(6). https://doi.org/10.1063/1.4725530.
[8] Watanabe T, Taniuchi T, Takano S, Aoki T, Fukami K. Permanent magnet based dipole magnets for next generation light sources. Phys Rev Accel Beams 2017;20 (7):072401.
[9] T.J. Burris-Mog et al. "Calibration of two compact permanent magnet spectrometers for high current electron linear induction accelerators," Rev Sci Inst 89 7 2018.
[10] Corvan DJ, Sarri G, Zepf M. Design of a compact spectrometer for high-flux MeV gamma-ray beams. Rev Sci Instrum 2014;85(6):065119. https://doi.org/10.1063/1.4884643.
[11] Chen H, et al. "High performance compact magnetic spectrometers for energetic ion and electron measurement in ultraintense short pulse laser solid interactionsa),". Rev Sci Inst 2008;79(10). https://doi.org/10.1063/1.2953679.
[12] Liang E, et al. High e+/e− ratio dense pair creation with 1021W. cm− 2 laser irradiating solid targets. Sci Rep 2015;5(1):13968.
[13] Sarri G, et al. Generation of neutral and high-density electron–positron pair plasmas in the laboratory. Nat Commun 2015;6(1):6747.
[14] Chen H, et al. "Magnetic collimation of relativistic positrons and electrons from high intensity laser–matter interactions,". Phys Plasmas 2014;21(4).
[15] Cowan TE, et al. High energy electrons, nuclear phenomena and heating in petawatt laser-solid experiments. Laser Part Beams 1999;17(4):773–83. https://doi.org/10.1017/S0263034699174238.
[16] Sarri G, et al. Laser-driven generation of collimated ultra-relativistic positron beams. Plasma Phys Controlled Fusion 2013;55(12):124017.
[17] Chen H, et al. Scaling the yield of laser-driven electron-positron jets to laboratory astrophysical applications. Phys Rev Lett 2015;114(21):215001.
[18] Sarri G, et al. Table-top laser-based source of femtosecond, collimated, ultrarelativistic positron beams. Phys Rev Lett 2013;110(25):255002.
[19] Fleck K, Cavanagh N, Sarri G. Conceptual design of a high-flux multi-GeV gamma-ray spectrometer. Sci Rep 2020;10(1):9894. https://doi.org/10.1038/s41598-020-66832-x.
[20] Cavanagh N, et al. Experimental characterization of a single-shot spectrometer for high-flux, GeV-scale gamma-ray beams. Phys Rev Research 2023;5(4):043046. https://doi.org/10.1103/PhysRevResearch.5.043046.
[21] Klein SR. e+e- Pair production from 10 GeV to 10 ZeV. Radiat Phys Chem 2006/06/01/ 2006,;75(6):696–711. https://doi.org/10.1016/j.radphyschem.2005.09.005.
[22] Tsai Y-S. Pair production and bremsstrahlung of charged leptons. Reviews of Modern Physics 1974;46(4):815–51. https://doi.org/10.1103/RevModPhys.46.815.
[23] Hough PVC. The angular distribution of pair-produced electrons and bremsstrahlung. Phys Rev 1948;74(1):80–6. https://doi.org/10.1103/PhysRev.74.80.
[24] Furlani EP. Permanent magnet and electromechanical devices: Materials, analysis, and applications. Elsevier Science; 2001.
[25] Tanabe JT. Iron dominated electromagnets: Design, fabrication. Assembly And Measurements: World Scientific Publishing Company; 2005.
[26] Noh Y, et al. Charge-neutral, GeV-scale electron-positron pair beams produced using bremsstrahlung gamma rays. Commun Phys 2024;7(1):44. https://doi.org/10.1038/s42005-024-01527-7.
[27] Kim H-I, et al. Electron-positron generation by irradiating various metallic materials with laser-accelerated electrons. Results Phys 2024;57:107310. https://doi.org/10.1016/j.rinp.2023.107310.
[28] Sung JH, et al. 4.2 PW, 20 fs Ti: sapphire laser at 0.1 Hz. Opt Lett 2017;42(11): 2058–61.
[29] Song H, et al. Characterization of relativistic electron–positron beams produced with laser-accelerated GeV electrons. Sci Rep 2023;13(1):310. https://doi.org/10.1038/s41598-023-27617-0.
[30] Dong Y, et al. Absolute x-ray calibration of an Amersham imaging plate scanner. Rev Sci Instrum 2020;91(3):033105. https://doi.org/10.1063/1.5140026.
[31] J. Won et al., "Monte Carlo Study of Imaging Plate Response to Laser-Driven Aluminum Ion Beams," Applied Sciences,11 (2) doi: 10.3390/app11020820.
[32] Boutoux G, et al. Study of imaging plate detector sensitivity to 5–18 MeV electrons. Rev Sci Inst 2015;86(11).
[33] Boutoux G, et al. Validation of modelled imaging plates sensitivity to 1–100 keV x-rays and spatial resolution characterisation for diagnostics for the "PETawatt Aquitaine Laser". Rev Sci Inst 2016;87(4).